ENZYME CATALYSIS AND REGULATION:

Metal Ion Binding and Coordination Geometry for Wild Type and Mutants of Metallo-β-lactamase from *Bacillus cereus* 569/H/9 (BcII): A COMBINED THERMODYNAMIC, KINETIC, AND SPECTROSCOPIC APPROACH

Dominique de Seny, Uwe Heinz, Sandra Wommer, Martin Kiefer, Wolfram Meyer-Klaucke, Moreno Galleni, Jean-Marie Frère, Rogert Bauer and Hans-Werner Adolph

J. Biol. Chem. 2001, 276:45065-45078.
doi: 10.1074/jbc.M106447200 originally published online September 10, 2001

THE JOURNAL OF BIOLOGICAL CHEMISTRY
Vol. 276, No. 48, Issue of November 30, pp. 45065–45078, 2001
Printed in U.S.A.

Metal Ion Binding and Coordination Geometry for Wild Type and Mutants of Metallo-β-lactamase from *Bacillus cereus* 569/H/9 (BcII)

A COMBINED THERMODYNAMIC, KINETIC, AND SPECTROSCOPIC APPROACH*

Received for publication, July 10, 2001, and in revised form, September 5, 2001
Published, JBC Papers in Press, September 10, 2001, DOI 10.1074/jbc.M106447200

Dominique de Seny,[a,b,c] Uwe Heinz,[b,d,e] Sandra Wommer,[d,f] Martin Kiefer,[d,g] Wolfram Meyer-Klaucke,[h] Moreno Galleni,[a] Jean-Marie Frère,[a] Rogert Bauer,[i,j] and Hans-Werner Adolph[d,k]

From the [a]Centre d'Ingéniérie des Protéines, Institut de Chimie B6, Université de Liège, Sart-Tilman, B-4000 Liège, Belgium, [d]FR 8.8 Biochemie, Universitaet des Saarlandes, D-66041 Saarbruecken, Germany, [h]European Molecular Biology Laboratory-Outstation Hamburg at Deutsches Elektronen-Synchrotron, Notkestrasse 85, D-22603 Hamburg, Germany, and [i]Department of Mathematics and Physics, The Royal Veterinary and Agricultural University, Thorvaldsensvej 40, DK-1871 Frederiksberg C, Denmark

One high affinity (nM) and one low affinity (μM) macroscopic dissociation constant for the binding of metal ions were found for the wild-type metallo-β-lactamase from *Bacillus cereus* as well as six single-site mutants in which all ligands in the two metal binding sites were altered. Surprisingly, the mutations did not cause a specific alteration of the affinity of metal ions for the sole modified binding site as determined by extended x-ray absorption fine structure (EXAFS) and perturbed angular correlation of γ-rays spectroscopy, respectively. Also UV-visible absorption spectra for the mono-cobalt enzymes clearly contain contributions from both metal sites. The observations of the very similar microscopic dissociation constants of both binding sites in contrast to the significantly differing macroscopic dissociation constants inevitably led to the conclusion that binding to the two metal sites exhibits negative cooperativity. The slow association rates for forming the binuclear enzyme determined by stopped-flow fluorescence measurements suggested that fast metal exchange between the two sites for the mononuclear enzyme hinders the binding of a second metal ion. EXAFS spectroscopy of the mono- and di-zinc wild type enzymes and two di-zinc mutants provide a definition of the metal ion environments, which is compared with the available x-ray crystallographic data.

Two zinc binding sites in close proximity are conserved in all metallo-β-lactamases studied so far. Only two of the metal ion ligands undergo variations between the three different subclasses of the enzyme family (1). The enzyme from *Bacillus cereus* 569/H/9 (BcII)[1] represents a member of subclass B1 with 3 His ligands in one site and 1 Asp, 1 Cys, and 1 His ligand in the other site (3H[1] and DCH[1] sites, respectively). Various crystal structures of BcII are available, representing mononuclear (2) and binuclear species (3, 4). It was shown earlier that both mono- and binuclear zinc enzymes from *B. cereus* (5) and *Bacteroides fragilis* (6) are catalytically active.

Although catalytic mechanisms for the enzyme with either one or two zinc ions bound have been discussed (for review see Ref. 7) the respective roles of the two binding sites during catalysis are still unclear. Generally the 3H site is considered to be the primary catalytic site. However, the importance of the DCH site for catalysis became obvious from studies of the C168A mutant. When only one zinc ion is bound to this mutant, it shows a very low activity compared with the wild type, whereas wild type-like activity is almost restored when a second metal ion is bound (5).

Perturbed angular correlation (PAC) of γ-ray spectroscopy provides information on the metal ion coordination geometry through measurement of the nuclear quadrupole interaction (NQI) between the nuclear electric quadrupole moment and the electric field gradient from the surrounding charge distribution. With this method it was possible to demonstrate that the Cd(II) ions in the mononuclear wild type BcII are distributed between the two metal binding sites (8). In a recent investigation combining PAC with ^{113}Cd-NMR spectroscopy, it was shown that the metal ions exchange between the two metal binding sites in a time regime of μs (9).

Extended x-ray absorption fine structure (EXAFS) spectroscopy of zinc proteins is unique in the sense that a direct observation of the zinc ion is possible (a detailed description of the method can be found in Ref. 10). In EXAFS spectroscopy the surroundings of a bound metal ion (absorber) are observed from the position of the metal ion, as in PAC and NMR spectroscopy. However, whereas the latter methods are sensitive to the angular position and the electrostatic properties of the ligands,

* The costs of publication of this article were defrayed in part by the payment of page charges. This article must therefore be hereby marked "*advertisement*" in accordance with 18 U.S.C. Section 1734 solely to indicate this fact.
[b] These authors contributed equally to the work.
[c] Supported by the Fonds pour la Formation à la Recherche dans l'Industrie et dans l'Agriculture.
[e] Supported by the Bundesministerium für Bildung und Forschung (contract 05SN8TSA1) and the Deutsche Forschungsgemeinschaft (Ad 152/1-2,3).
[f] Supported by the European research network on metallo-β-lactamases, within the Training and Mobility of Researchers program (CT 98-0232).
[g] Supported by the Deutsche Forschungsgemeinschaft (Ad 152/1-2).
[j] Supported by the Danish Natural Science Research Council.
[k] To whom correspondence should be addressed. Tel.: 49-681-3022492; Fax: 49-681-3022097; E-mail: hwadolph@mx.uni-saarland.de.

[1] The abbreviations used are: BcII, metallo-β-lactamase from *Bacillus cereus*; PAC, perturbed angular correlation of γ-rays; EXAFS, extended x-ray absorption fine structure; CcrA, metallo-β-lactamase from *Bacteroides fragilis*; 3H site, zinc binding site composed of three histidine residues; DCH site, zinc binding site composed of asparagine, cysteine, and histidine; NQI, nuclear quadrupole interaction; LMCT, ligand-to-metal charge transfer, MF, Mag-fura-2; d-d transition, ligand-field electronic transition.

the intensity of back-scattering depends mainly on the number of electrons in the back-scattering atom and the distance to the absorber. Defined patterns obtained from multiple scattering, including atoms more distant than the first coordination sphere, allow the identification of histidines as ligands (for a description of the method see Ref. 11 and references therein). For a given model, EXAFS spectroscopy predicts absorber-ligand distances with a precision unmatched by protein crystallographic measurements and thereby represents a method to refine the geometry of a known absorber site.

To probe the role of all six protein ligands of the metal ions in BcII, we produced the following mutants: H86S, H88S, and H149S in the 3H site and D90N, C168S, and H210S in the DCH site. To study the effects on metal ion binding we prepared the metal-free enzymes and determined the affinities for zinc, cobalt, and cadmium. We used stopped-flow fluorescence measurements to study the kinetics of metal ion binding to the wild type enzyme and UV-visible spectroscopy to characterize the cobalt-substituted enzymes. Zinc binding was studied by EXAFS spectroscopy to allow conclusions concerning modification of bond lengths and ligand composition, whereas PAC spectroscopy was used to probe an eventual distribution of Cd(II) in a mono-Cd(II) species of the H88S mutant enzyme.

MATERIALS AND METHODS

Site-directed Mutagenesis, Production, and Purification of Enzyme Species—Site-directed mutagenesis of the *B. cereus* 569/H/9 metallo-β-lactamase gene was performed with the help of the QuickChange site-directed mutagenesis kit. The mutations were performed in pCIP102. The desired mutants were identified by DNA sequencing on minipreps. The BcII genes containing the mutation were cloned into the pET9a plasmid. The different mutated genes were isolated from pCIP102 by digestion with the restriction enzymes *Nde*I and *Bam*HI. They were cloned into pET9a digested with the same enzymes to yield pCIP103-H116S, pCIP103-H118S, pCIP103-H196S, pCIP103-H263S, and pCIP103-D102N (new numbering of amino acids according to Ref. 1). The C168A and C168S mutants were produced and purified as described (5). All of the other mutants were expressed in *Escherichia coli* BL21(DE3) as soluble intracellular proteins. They were purified as described (5). The purity and the molecular masses of all purified proteins were confirmed by electrospray mass spectrometry. Further details of production and characterization will be published elsewhere together with a detailed analysis of protein stability, pH, and substrate profiles of the mutant enzymes.[2]

Production and Characterization of Metal-free Enzymes—The protein concentrations were determined by measuring the absorbance at 280 nm using an extinction coefficient of 30500 M^{-1} cm^{-1} for WT BcII and all mutants except C168A, for which a value of 31000 M^{-1} cm^{-1} was used. Zinc concentrations in samples and in the final dialysis buffers were determined by atomic absorption spectroscopy in the flame mode as described (12).

To produce "metal-free" buffers, buffer solutions in bi-distilled water were treated by extensive stirring with Chelex 100 (Sigma). Apo-enzymes were prepared by dialysis of the corresponding enzymes against two changes of 15 mM HEPES, pH 7.0, containing 0.2 M NaCl and 20 mM EDTA over a 12-h period under stirring. EDTA was removed from the resulting apoenzyme solution by three dialysis steps against the same buffer containing 1 M NaCl and Chelex-100 and finally two dialysis steps against 15 mM HEPES, pH 7.0, containing 0.2 M NaCl and Chelex-100. In all preparations the residual zinc content did not exceed 5% as determined by atomic absorption spectroscopy.

Reactivation of the apo-enzymes was studied with 100 μM Imipenem (Merck Sharp and Dohme, Bruxelles, Belgium) as the substrate in presence of 100 μM Zn(II) in 10 mM HEPES, pH 7.0, containing 0.2 M NaCl. Initial rates were determined using $\Delta A_{300\ nm} = -9000\ M^{-1}\ cm^{-1}$. All apo-enzymes could be reactivated, resulting in activities of 65–85% of the expected values.

Determination of Metal Ion Affinities—The dissociation constants for a first (*K*(mononuclear)) and second (*K*(binuclear)) zinc or cadmium ion bound were obtained from competition experiments with the chromophoric chelator Mag-fura-2 (MF; Molecular Probes, Eugene, OR). The indicator was titrated with metal in absence and presence of apo-enzyme (protein/indicator ratios were between 1:1 and 1:3) monitoring changes in absorbance at 363 nm.

The program Chemsim (developed by R. Kramer, Saarbruecken, Germany) was used for numerical data analysis. The program allows analysis of binding experiments involving arbitrary combinations of coupled equilibria (13). For calculations involving coupled equilibria, a combination of a Simplex algorithm with a Newton-Raphson procedure was used to minimize the sum of least squares. A data file for the experiments described here contains the total absorbance measured as a function of added volume of a metal ion stock solution of known concentration to a defined starting volume. Simulated absorbance values are calculated numerically for each titration step as the sum of relative contributions of contributing compounds (*e.g.* $A_{total} = \epsilon_{MF}[MF] + \epsilon_{Me\text{-}MF}[Me\text{-}MF]$). Starting concentrations of compounds, absorption coefficients and dissociation constants can undergo iterative optimization in arbitrary combinations. Therefore, equations are generated that include the laws of mass action, the ionic product of water (if necessary), and the equations for mass conservation. The number of equations is in all cases equal to the number of species in the simulated system. From simultaneous fittings of dissociation constants, absorption coefficients, and apo-enzyme concentrations, these values could be obtained with high precision and were used for calculations of all enzyme concentration-dependent parameters.

The following equilibria were used for fitting.

$$\text{Me-MF} \xleftrightarrow{K(\text{Me-MF})} \text{Me} + \text{MF} \qquad K(\text{Me-MF}) = \frac{[\text{Me}][\text{MF}]}{[\text{Me-MF}]} \qquad \text{(Eq. 1)}$$

$$\text{Me-BcII} \xleftrightarrow{K(\text{mononuclear})} \textit{Me} + \text{apo-BcII}$$

$$K(\text{mononuclear}) = \frac{[\text{Me}][\text{apo-BcII}]}{[\text{Me-BcII}]} \qquad \text{(Eq. 2)}$$

$$\text{Me}_2\text{-BcII} \xleftrightarrow{K(\text{binuclear})} \textit{Me} + \text{Me-BcII}$$

$$K(\text{binuclear}) = \frac{[\text{Me}][\text{Me-BcII}]}{[\text{Me}_2\text{-BcII}]} \qquad \text{(Eq. 3)}$$

The dissociation constant obtained for the Zn(II)-Mag-fura-2 complex was 81 (± 5) nM with $\epsilon_{MF,\ 363\ nm} = 28{,}500\ M^{-1}\ cm^{-1}$, slightly deviating from the reported values (14) obtained under different conditions. For Cd(II), $K_{Cd\text{-}MF} = 126$ (± 12) nM resulted (see Fig. 1).

The UV-visible bands of the Co_1 enzymes were used to estimate the dissociation constants directly from the spectroscopic data using numerical fitting of a one-step binding model (Equation 2).

Fluorescence Spectroscopy Used to Determine Metal Ion Binding Kinetics to Metal-free BcII Wild Type—Kinetics of Zn(II), Cd(II), and Co(II) binding could be followed by monitoring metal ion-induced changes of protein fluorescence. The experiments were performed with a DX17.MV stopped-flow spectrofluorimeter (Applied Photophysics). Two consecutive processes could be observed at high metal ion concentrations requiring a two-step binding model for data analysis. Only for the binding of Cd(II) were the rate constants of both processes so different that the two phases could each be treated as independent pseudo-first order reactions. From fits of mono-exponential functions to both phases with two different time intervals (see Fig. 4*B*), a dependence of apparent rate constants (k_{app}) on the metal ion concentration ([Me]) was found that could be interpreted according to Equation 4 for total metal ion concentrations much larger than the total enzyme concentration.

$$k_{app} = k_{on}[\text{Me}] + k_{off} \qquad \text{(Eq. 4)}$$

Binding of Co(II) resulted in biphasic reaction traces, which were evaluated by fitting bi-exponential functions to the data. Because both phases occurred with k_{app} values deviating by less than 1 order of magnitude and the second phase showed only about 20% of the amplitude of the first more rapid phase, only the first rate constant could be obtained with reliability. For Zn(II) binding, the amplitude of the second reaction phase was too low to allow data evaluation (see Fig. 4*E*); therefore only the first binding process resulted in a reliable association rate constant.

[2] D. de Seny, C. Prosperi-Meys, C. Bebrone, M. I. Page, J.-M. Frère, and M. Galleni, manuscript in preparation.

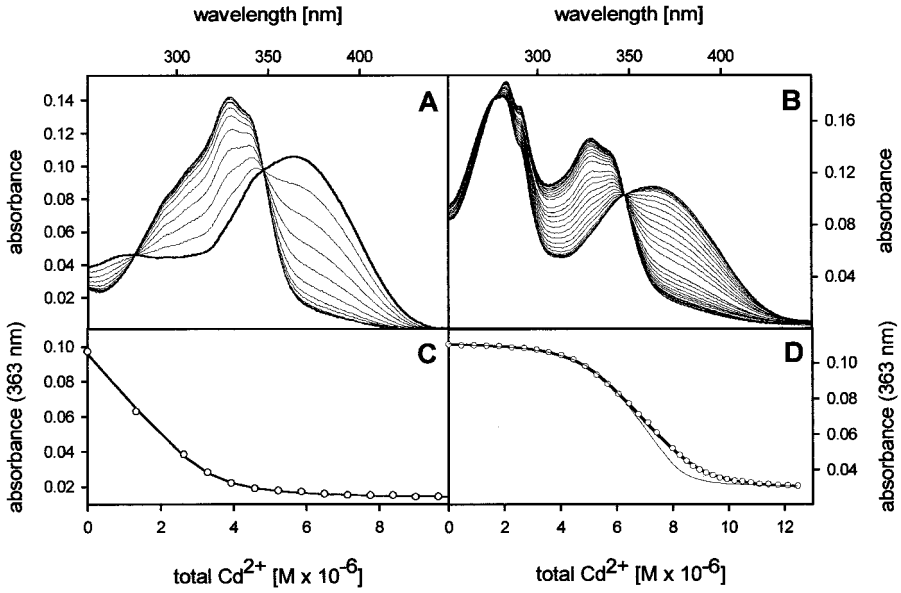

FIG. 1. **Determination of the affinity of the H88S BcII mutant for Cd(II) by competition with Mag-fura-2.** *A*, titration of 3.37 μM Mag-fura-2 in 15 mM HEPES, pH 7.5, containing 0.1 M NaCl with 250 μM Cd(II) at 25 °C. The resulting spectra were adjusted for small corrections in dilution during the titration and normalized at the isosbestic point at 342 nm. *B*, titration of a solution containing 3.88 μM Mag-fura-2 and 4.95 μM metal-free BcII H88S enzyme in 15 mM HEPES, pH 7.5, containing 0.1 M NaCl with Cd(II). *C*, the absorbance change at the maximum of the zinc-free compound (*thick line* in *A*) at 363 nm was used for fitting a one-step binding model (Equation 1) to the data resulting in $\epsilon_{363\ nm}$ = 28500 M^{-1} cm^{-1}, and a dissociation constant for the Cd·Mag-fura-2 complex of $K_{Cd\text{-}MF}$ = 126 nM. *D*, the absorbance change at 363 nm (*open circles*) was used for numerical fitting (*thick line*) of coupled equilibria (Equations 1–3), constraining the extinction coefficient and the dissociation constant of Cd·Mag-fura-2 to the values obtained in *C*. The average dissociation constants obtained from repeated experiments are listed in Table I. The exclusive consideration of formation of a Cd_1-enzyme complex (only Equations 1 and 2 were used for fitting) resulted in systematic deviations of the calculated titration curves from the data. This feature was present in all repeated experiments and also for zinc titrations with all enzyme species. An alternative fit of a one-step binding model (Equations 1 and 2) to a data set in which all data points between 6 and 11 μM total Cd(II) were omitted was performed (*thin line*). The resulting high affinity dissociation constant is equal to that with the two-step binding model, but saturation of MF is reached at a lower Cd(II) concentration; this underlines that a second low affinity binding of Cd(II) to the enzyme has to be taken into account in the second bend phase of the titration.

Extended X-ray Absorption Fine Structure (EXAFS) Spectroscopy on the Zn edge in BcII—The Zn K-edge was monitored at beam line D2 at DESY/Hamburg running at 4.5-GeV and 70–125-mA current in fluorescence mode. Standard EXAFS analysis was performed using the EXPROG software package[3] to process the raw data and EXCURV98[4] using exact curve wave single scattering theory (15, 16) to analyze the spectra. Phases were calculated *ab initio* using Hedin-Lundqvist potentials and von Barth ground states (17). Both single and multiple scattering paths up to 4.5 Å from the metal atom were used to identify and quantify imidazole coordination of histidine ligands.

The fitting process included constraints for the following parameters. The energy range was set to 30–650 eV above the edge. Two coordination clusters were introduced, each having an integer number of ligands. The fit then determined the fractional occupancy of each cluster for the mononuclear enzyme if the metal ions were distributed between the two metal sites. For the binuclear case, the occupancy of the two clusters was fixed to 0.5. Theoretical fits were generated by adding shells of scatterers around the central zinc atoms and iterating the number of scatterers, bond lengths, and Debye-Waller factors in each shell. Additionally, the Fermi energy, EF (edge position relative to calculated vacuum position), was iterated to achieve the best fit to the experimental data. The improvement of the fit after the addition of each additional shell beyond the first was assessed by comparing the residual *R*-factor (18).

Distances and Debye-Waller factors of the outer shell atoms of imidazole rings were constrained assuming the Debye-Waller factors of atoms with similar distance to the absorber to be equal. Because the constraints for the Debye-Waller factors are unique for each parameter set, the details are summarized in Table II.

Perturbed Angular Correlation of γ-Ray Spectroscopy—^{111m}Cd was produced by the Cyclotron Department at the University Hospital in Copenhagen. Preparation and purification of ^{111m}Cd is described in Ref. 19. The PAC spectrometer is described in Ref. 20 and references therein.

[3] Developed by C. Hermes and H. F. Nolting at the EMBL-Outstation, Hamburg, Germany.

[4] Developed by N. Binsted, S. W. Cambell, S. J. Gurman, and P. Stephenson, Daresbury Laboratory, UK.

In the case of identical, static and randomly oriented molecules, the perturbation function $G_2(t)$ is as shown in Equation 5,

$$G_2(t) = a_0 + a_1 \cos(\omega_1 t) + a_2 \cos(\omega_2 t) + a_3 \cos(\omega_3 t) \qquad \text{(Eq. 5)}$$

with ω_1, ω_2, and ω_3 as the three difference frequencies between the three sublevels of the spin 5/2 state of the cadmium nucleus (21). Note that $\omega_1 + \omega_2 = \omega_3$. Thus, the Fourier transform of $G_2(t)$ exhibits three frequencies for each NQI. The Fourier transformation was performed as described (20). The NQI is described by the numerically largest diagonal element after diagonalization, chosen as ω_{zz}, which is denoted ω_0 and $\eta = (\omega_{xx} - \omega_{yy})/\omega_{zz}$. The relationship between these two parameters and the frequencies in $G_2(t)$ can be found in Ref. 21. Thus, from the time dependence of $G_2(t)$, ω_0 and η, determined through least squares fitting, reflect the coordination geometry of the cadmium ion.

In the liquid state the NQI is time-dependent because of the Brownian reorientation of the protein, described by the rotational diffusion time, τ_R. Consequently, $G_2(t)$ converges to 0 as a function of time, representing thermal equilibrium and isotropy in the angular correlation between the two γ-rays.

The perturbation function, $A_2G_2(t)$, where A_2 is the amplitude, was analyzed by a conventional nonlinear least squares fitting routine. Satisfactory fitting was obtained with a relative Gaussian distribution, $\delta = \Delta\omega_0/\omega_0$, applied to all of the three frequencies. Non-zero values for δ indicate a distribution of the ^{111m}Cd nuclei among different surroundings. A NQI is then described by the parameters ω_0, η, δ, and τ_R. In cases where more than a single NQI is present, the perturbation function is the sum of the different perturbation functions, where each NQI is weighted by its population (20).

RESULTS

Macroscopic Dissociation Constants of Zinc and Cadmium Complexes—We performed competition experiments with the chromophoric chelator Mag-fura-2 for the determination of dissociation constants for zinc and cadmium ions to the metal-free enzymes. The titration data for the chelator MF with Cd(II) ions are shown in Fig. 1*A*. The spectra show an isosbestic point

TABLE I

Dissociation constants of Me_1 and Me_2 species of wild type and mutant BcII

Data for Zn(II) and Cd(II) binding were obtained from competition titrations with Mag-fura-2 as described under "Materials and Methods." Dissociation constants for Co(II) complexes were derived from spectral changes of the enzyme upon Co(II) binding. *K*(mononuclear) and *K*(binuclear) represent the macroscopic dissociation constants of the Me-BcII and Me_2-BcII complexes, respectively; ND, not determined.

Enzyme species	*K*(mononuclear)			*K*(binuclear)		
	Zn(II)	Cd(II)	Co(II)	Zn(II)	Cd(II)	Co(II)
	nM	*nM*	*μM*	*μM*	*μM*	*μM*
Wild type	0.62 (± 0.08)	8.3 (± 0.5)	0.093 (± 0.015)	1.50 (± 0.71)	5.9 (± 1.0)	66.7 (± 10.0)
H86S	5.30 (± 2.34)	ND	10.5 (± 1.5)	0.32 (± 0.11)	ND	ND
H88S	0.38 (± 0.15)	3.8 (± 0.3)	9.1 (± 1.1)	1.13 (± 0.19)	1.4 (± 0.1)	ND
H149S	3.11 (± 0.05)	ND	2.7 (± 0.3)	0.19 (± 0.02)	ND	ND
D90N	2.00 (± 0.39)	ND	20.0 (± 3.5)	5.02 (± 2.39)	ND	ND
C168S	0.61 (± 0.19)	ND	3.1 (± 0.4)	2.34 (± 0.59)	ND	ND
C168A	ND	ND	1.1 (± 0.1)	ND	ND	ND
H210S	0.43 (± 0.11)	ND	0.35 (± 0.05)	2.53 (± 0.50)	ND	ND

at 270 nm and maxima at 363 and 330 nm for the metal-free compound and the 1:1 cadmium complex, respectively. Fig. 1, *B* and *D*, represents Cd(II) binding to the H88S mutant as a typical example of the experimental data and fitting.

Fitting a one-step binding model (Equations 1 and 2) to the data resulted in unsatisfactory residuals for all enzyme species tested. As no change in absorbance occurs before a concentration of about 2 μM Cd(II) ions is reached (Fig. 1*D*), the enzyme has a higher affinity for cadmium than MF. In the end phase of the titration additional competition with MF for the binding of a second metal ion to the enzyme must occur, because saturation of the chelator needs higher concentrations of metal than expected for a one-step binding model (*thin line* in Fig. 1*D*). Thus a binding model with two equilibria for subsequent formation of Me_1 and Me_2 enzyme should be used for fitting (Equations 1–3). The resulting dissociation constants are summarized in Table I. All enzyme species investigated show a high and a low affinity macroscopic dissociation constant corresponding to high affinity for binding a first zinc or cadmium ion and significantly weaker affinity for binding a second ion. The high and low affinity macroscopic dissociation constants for the different enzyme samples differ generally by less than two orders of magnitude from the dissociation constants of the Me-MF complex. Thus, a sufficiently high data point density in both bend regions of the titration curves allowed the simultaneous determination of both dissociation constants with statistical reliability.

Absorption Spectroscopy and Binding of Co(II) to Wild Type and Mutant Enzymes—Binding of Co(II) to the metal-free wild type enzyme results in the appearance of a ligand-to-metal charge transfer (LMCT) band at 344 nm and additional absorption bands in the visible range, due to d-d transitions. Fig. 2 demonstrates that the wild type enzyme can bind two equivalents of Co(II), resulting in a second LMCT band at 383 nm. The appearance of the different bands during titration was used to determine the dissociation constants of the Co(II) species. Again a two-step binding model was necessary to account for the data obtained with the wild type. The changes at the different band positions could be fitted with the same set of dissociation constants, yielding the extinction coefficients of the different bands (see *inset* of Fig. 2).

Titrations of the metal-free mutant enzymes were performed as described above (Fig. 2). Binding of a second Co(II) ion to the mutant species was generally difficult to determine because of weak binding and an observed instability of the proteins in the presence of high concentrations of Co(II), which led to precipitation of the enzymes. Thus, only the Co_1 species are described here. Fig. 3 represents normalized spectra such that the extinction coefficients are shown as the ordinates. The *insets* represent titrations and corresponding fits performed at specific wavelengths for each mutant from which we derived the dissociation constants (Table I). The normalization of the spectra is based on the enzyme concentrations and extinction coefficients obtained from the fits.

Kinetics of Metal Ion Binding to BcII Wild Type—We observed that binding of Zn(II), Cd(II), and Co(II) modified the fluorescence intensity when monitoring the protein fluorescence of BcII. The change in amplitude induced by Zn(II) or Cd(II) binding was small compared with the total fluorescence but intense enough to allow monitoring of metal ion binding kinetics. For all three metal ions, biphasic kinetics resulted. In the case of Co(II) binding, the protein fluorescence was quenched in two consecutive steps. Because of the data quality only the first phase of Co(II) association could be used for accurate determination, resulting in $k_{on,1} = 0.28\ \mu M^{-1}\ s^{-1}$ (Fig. 4*C*). The second phase is characterized by an association rate around $0.03\ \mu M^{-1}\ s^{-1}$. For Cd(II) rapid metal ion binding resulted in fluorescence quenching followed by a second slower phase at [Cd(II)]/[enzyme] > 1 leading to a fluorescence increase (Fig. 4, *A* and *B*). The two phases could be fitted separately with mono-exponential functions resulting in k_{app} values, which were found to depend linearly on the metal ion concentration (Cd(II)/E ≫ 1) giving $k_{on,1} = 26\ \mu M^{-1}\ s^{-1}$ and $k_{on,2} = 0.5\ \mu M^{-1}\ s^{-1}$ (Fig. 4*C*). Binding of Zn(II) quenched the protein fluorescence in a rapid first phase. In a second phase, a small recovery of protein fluorescence occurred (Fig. 4, *D* and *E*). Only the first phase of the reaction gave useful data for the determination of an association rate constant ($k_{on,1} = 14\ \mu M^{-1}\ s^{-1}$) (Fig. 4*F*). Because of the low signal/noise ratio, the second association rate constant could only be estimated to below 1 $\mu M^{-1}\ s^{-1}$. Combining the association rates with the corresponding dissociation constants (Table I) we obtained the following dissociation rates for the wild type enzyme: $k_{off,1} = 0.22\ s^{-1}$ and $k_{off,2} = 3.0\ s^{-1}$ for Cd(II); $k_{off,1} = 0.0087\ s^{-1}$ and $k_{off,2} < 1.5\ s^{-1}$ for Zn(II); and $k_{off,1} = 0.026\ s^{-1}$ for Co(II).

EXAFS Spectroscopy Measured on the Wild Type and Mutant Enzymes—To characterize the differences between the Zn_1 and Zn_2 enzymes we investigated both species. The Zn_1 wild type

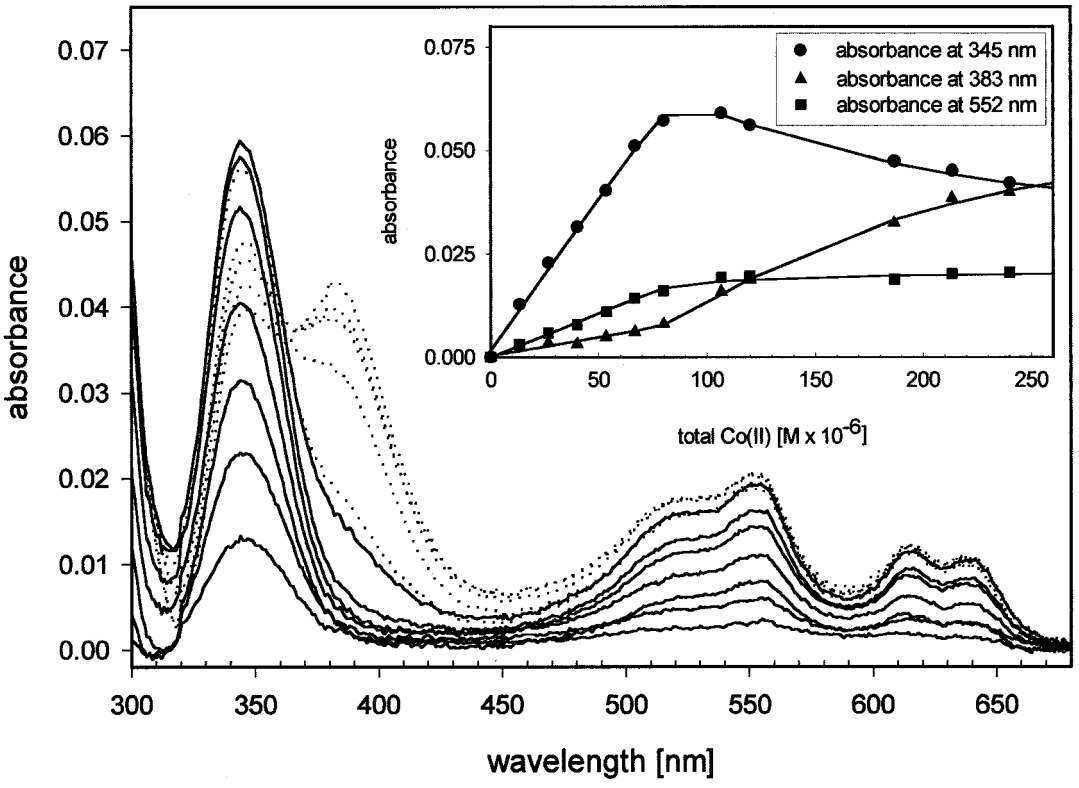

FIG. 2. **Titration of metal-free BcII wild type with Co(II).** A solution of 85 μM metal-free wild type BcII in 15 mM HEPES, pH 7.5, was titrated with a 2 mM Co(II) stock solution. The spectra representing mainly the binding of a first equivalent of Co(II) are presented as *solid lines* and spectra corresponding to binding of a second equivalent of Co(II) as *dotted lines*. The *inset* shows the absorbance increase at the different band maxima (*symbols*) and corresponding fits (*lines*) of a sequential two-step binding model (Equations 2 and 3) using numerical simulation with the program Chemsim. The same set of dissociation constants could be used for fitting for all band positions. The extinction coefficients obtained for the Co_1 enzyme are $\epsilon_{344\ nm}$ = 760 M^{-1} cm^{-1}, $\epsilon_{552\ nm}$ = 210 M^{-1} cm^{-1}, $\epsilon_{614\ nm}$ = 116 M^{-1} cm^{-1}, and $\epsilon_{640\ nm}$ = 100 M^{-1} cm^{-1}. The resulting dissociation constants are listed in Table I.

enzyme was produced by adding 1 equivalent of zinc ions to the metal-free enzyme before concentrating the sample. Atomic absorption spectroscopy gave a calculated zinc content of 1.1 equivalents/enzyme molecule, whereas the Zn_2 enzyme contained two zinc ions. The resulting spectra are compared in Fig. 5. The samples of the mutant enzymes were prepared from solutions containing 100 μM zinc. The exchange of 15 mM HEPES for BisTris was performed by iterative ultrafiltration with Centricon devices. Data evaluation of the EXAFS spectra suggested the formation of the Zn_2 species for both the C168S and the H210S mutants. The corresponding spectra are shown in Fig. 5. The results of fitting of the EXAFS spectra are summarized in Table II.

PAC Spectroscopy of the Cd(II)-H88S Mutant—We obtained a PAC spectrum from the H88S mutant in 55% sucrose, 50 μM enzyme, 0.1 M NaCl, pH 7.1, and 0.2 equivalents Cd(II) ions relative to the enzyme at 1 °C (see Fig. 6). It did not give any indication of the presence of free cadmium and clearly exhibited two NQIs with amplitudes of 30 and 70% of the total signals. The spectroscopic parameters obtained are summarized in Table III and compared with earlier published data on the wild type enzyme and the C168A mutant.

DISCUSSION

Although different mechanisms for mono- and binuclear metallo-β-lactamases have been discussed in the literature, it is still not clearly understood why the enzymes have two conserved zinc binding sites (for review see Ref. 7). The mononuclear mechanism proposed (22) predicts that the so-called first binding site, composed of 3 His residues in subclass B1 (3H site), is the site responsible for catalytic activity. However, this mechanism does not take into account the fact that the DCH site could be of functional importance. The basis for the present investigation was the need to identify the role of both binding sites through a systematic replacement of all the zinc ligands by hydrophilic residues, with an expected weaker capacity for zinc binding. Serine was chosen to replace the histidines and cysteine, whereas Asp^{90} was replaced by Asn to remove the negative charge while leaving the occupied space almost conserved.

The representation of the substrate binding site in Fig. 7 shows that the side chains of all the zinc ligands but His^{86} contribute to the definition of the surface of the substrate binding pocket. If one excepts this residue, all substitutions result in a drastic change either of the electrostatics of the active site (D90N) or of the available space in the catalytic center of the enzyme. The D90N substitution was considered important because the negative charge of the carboxylate group compensates the positive charge of the neighboring Arg^{91} side chain in a distance of 2.9 Å as derived from the coordinate file, 1BVT (3).

Binding of Zinc and Cadmium Ions—When studying the affinities of the various enzyme species for zinc and cadmium in competition with the chromophoric chelator Mag-fura-2 (see Fig. 1), we found that data evaluation required two protein-specific equilibria describing the formation of Me_1 and subsequently of Me_2 species (Table I), characterized by a high and a low affinity macroscopic dissociation constant. Only minor modifications of the macroscopic dissociation constants are observed when the mutant and the wild type enzymes are compared. Although we expected that the mutants would exhibit a strong preference for the occupation of the unmodified site, the

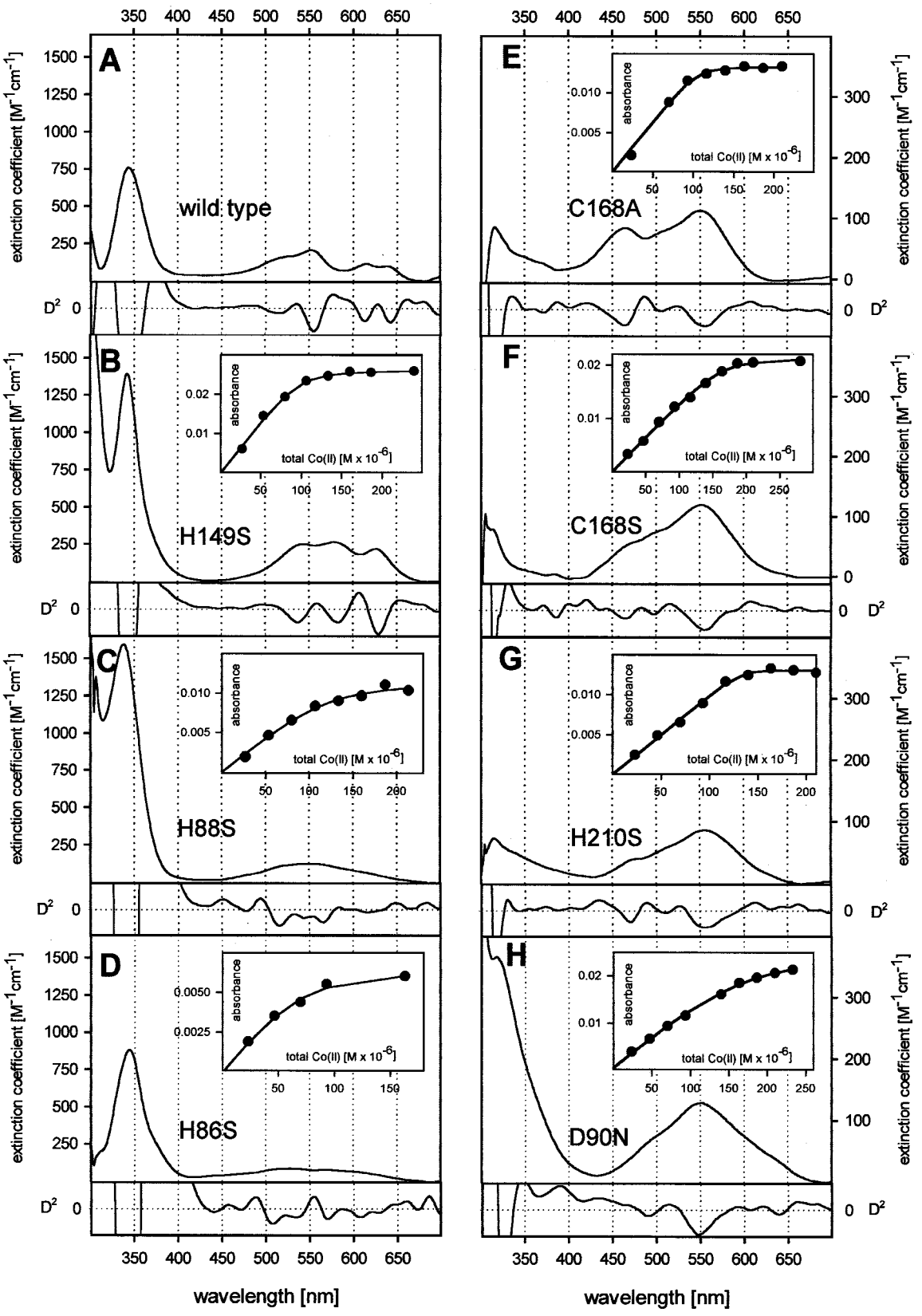

FIG. 3. **UV-visible spectra of Co(II)-substituted native and mutant BcII.** The UV-visible spectra of the apo-enzymes (80–200 μM) in 15 mM HEPES, pH 7.5, containing 0.2 M NaCl upon titration with Co(II) ions were recorded at 25 °C. The different panels show spectra of the Co_1 enzymes normalized to 1 M concentrations, thus representing the extinction coefficients as the ordinates. The *insets* represent titrations of the metal-free enzymes with a 4 mM stock solution of Co(II). Data are shown as *filled circles* representing the absorbance at the wavelengths given below. *Lines* represent fits obtained from numerical simulation of a one-step binding model to the data using the program Chemsim (see "Materials and Methods"). The equilibrium constant (see Table I), enzyme concentration, and extinction coefficient at the monitored band positions were optimized simultaneously. Enzyme concentrations obtained from the fits were used to normalize the spectra. Third order Savitzki-Golay smoothing of normalized spectra was performed such that neither band positions nor total absorptions were modified. The smoothed spectra were used to calculate second derivatives, which are presented *below* each spectrum (D^2) to facilitate localization of bands and shoulders appearing as the

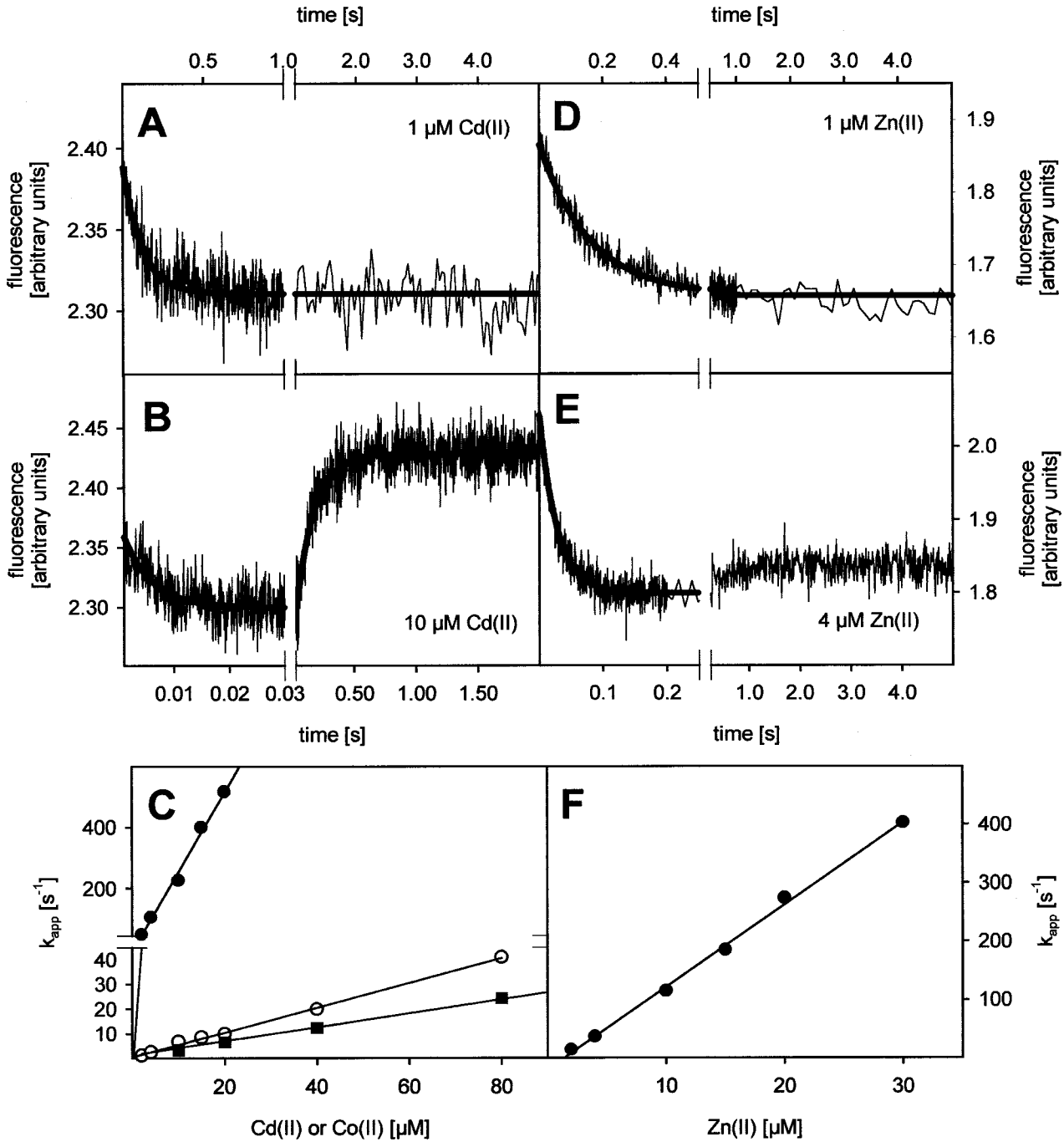

FIG. 4. **Kinetics of metal ion binding to BcII.** Binding of Zn(II), Cd(II), and Co(II) was monitored by changes of protein fluorescence resulting from metal ion binding. Metal-free enzyme (1 μM after mixing) was mixed with equal volumes of buffer containing different concentrations of metal ions (0.5–1000 μM after mixing) in 20 mM sodium cacodylate, pH 7.0. The excitation wavelength was 280 nm, and fluorescence emission was detected above 320 nm using a cutoff filter in the emission light path. To improve the signal-to-noise ratio, 5–10 reaction traces were averaged. Up to a [metal]/[enzyme] ratio of 1 the reaction traces were monophasic, showing a quenching of protein fluorescence. At metal/enzyme ratios > 1, a second slower reaction phase was observed, characterized by a fluorescence increase in case of Cd(II) (*B*, 10 μM Cd(II)) and Zn(II) (*E*, 4 μM Zn(II)). Mono-exponential fits to the first reaction phase (*A, B, D,* and *E*) and to the second reaction phase (*B*) are shown as *thick lines*. *C*, apparent rate constants for the first (*filled circles*) and second (*open circles*) reaction phases of Cd(II) binding. Linear regression analysis (*lines*) resulted in $k_{on,1}$ = 26.0 ($\pm$ 1.3) μM^{-1} s^{-1} for the first and $k_{on,2}$ = 0.50 ($\pm$0.01) μM^{-1} s^{-1} for the second phase. The corresponding data for the first phase of Co(II) binding are shown as *filled squares*, resulting in $k_{on,1}$ = 0.28 ($\pm$0.01) μM^{-1} s^{-1}. *F*, linear regression analysis (*line*) of apparent rate constants for the first phase of Zn(II) binding (*filled circles*) resulted in $k_{on,1}$ = 14.1 ($\pm$ 0.3) μM^{-1} s^{-1}.

minima in the derivative spectra. Difference spectra were obtained by subtracting the UV-visible spectrum of the apo-β-lactamase from those of the metal-substituted forms after normalization for protein and metal concentration if necessary. *A*, Co_1-wild type BcII calculated from the spectrum in Fig. 2 having [enzyme] = 85 μM and [Co(II)] = 50 μM. *B*, Co_1-H149S mutant ($\epsilon_{342\ nm}$ = 1400 M^{-1} cm^{-1}, $\epsilon_{543\ nm}$ = 252 M^{-1} cm^{-1}, $\epsilon_{578\ nm}$ = 267 M^{-1} cm^{-1}, $\epsilon_{627\ nm}$ = 221 M^{-1} cm^{-1}). *Inset*, titration of 98 μM enzyme with Co(II) at 578 nm. *C*, Co_1-H88S mutant ($\epsilon_{338\ nm}$ = 1596 M^{-1} cm^{-1} and $\epsilon_{546\ nm}$ = 124 M^{-1} cm^{-1}). *Inset*, titration of 122 μM enzyme with Co(II) at 550 nm. *D*, Co_1-H86S mutant ($\epsilon_{344\ nm}$ = 884 M^{-1} cm^{-1}, $\epsilon_{530\ nm}$ = 84 M^{-1} cm^{-1} and $\epsilon_{570\ nm}$ = 76.6 M^{-1} cm^{-1}). *Inset*, titration of 80 μM enzyme with Co(II) at 533 nm. *E*, Co_1-C168A mutant ($\epsilon_{466\ nm}$ = 84.5 M^{-1} cm^{-1} and $\epsilon_{553\ nm}$ = 112.8 M^{-1} cm^{-1}). *Inset*, titration of 120 μM enzyme with Co(II) at 550 nm. *F*, Co_1-C68S mutant ($\epsilon_{553\ nm}$ = 120 M^{-1} cm^{-1}). *Inset*, titration of 188 μM enzyme with Co(II) at 554 nm. *G*, Co_1-H210S mutant ($\epsilon_{555\ nm}$ = 86.3 M^{-1} cm^{-1}). *Inset*, titration of 151 μM enzyme with Co(II) at 556 nm. *H*, Co_1-A90A mutant ($\epsilon_{551\ nm}$ = 129 M^{-1} cm^{-1}). *Inset*, titration of 197 μM enzyme with Co(II) at 550 nm.

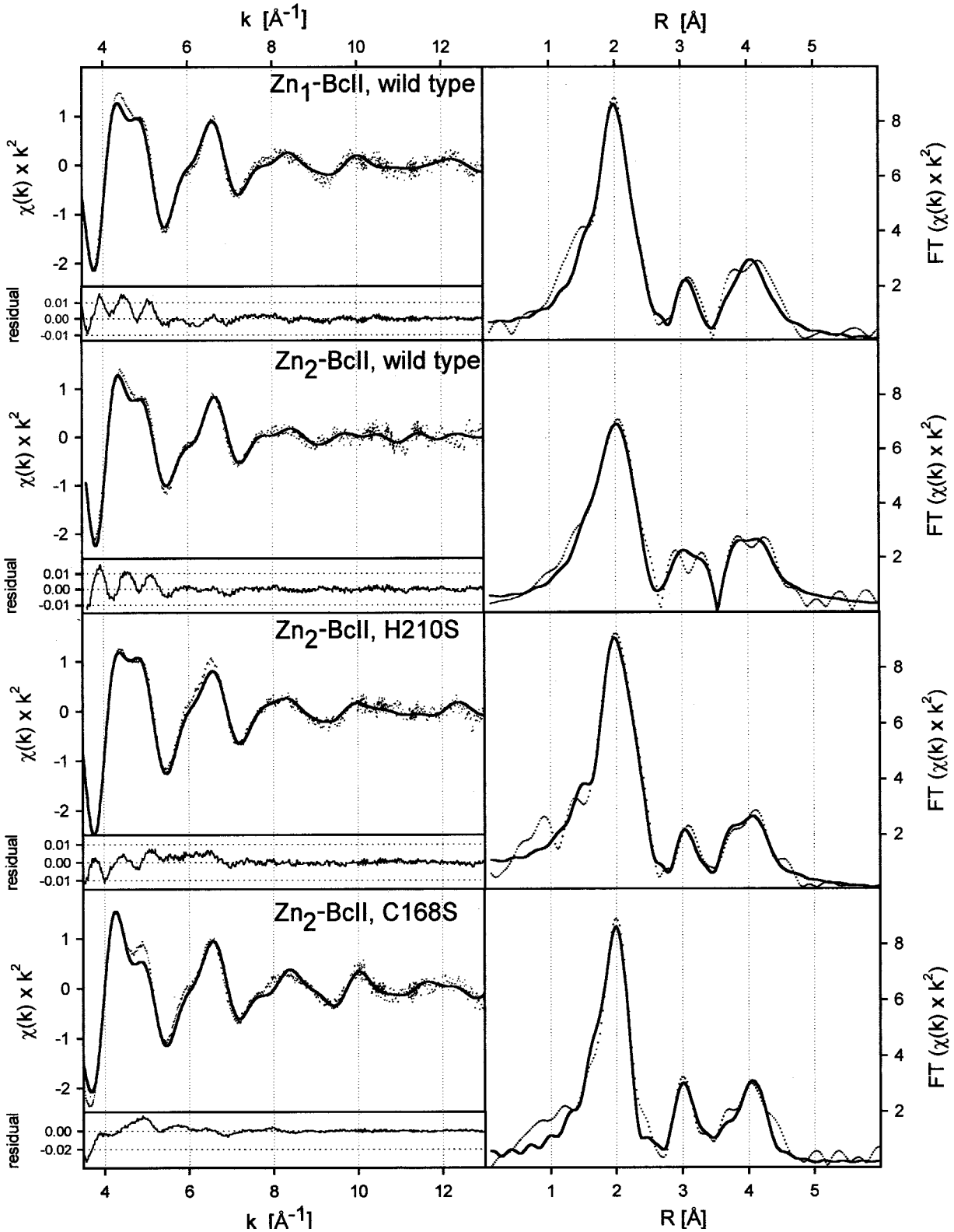

FIG. 5. **Fitting of EXAFS results for Zn_1- and Zn_2-BcII wild type and Zn_2-BcII mutants H210S and C168S.** The k^2-weighted EXAFS spectra (*dotted line*) with the theoretical fits (*solid line*) are shown to the *left* together with the residuals ($(\chi(k)k^2)_{\text{experimental}} - (\chi(k)k^2)_{\text{theoretical}}$). The corresponding Fourier transforms in *R*-space (experimental data and fit are represented by a *dotted line* and a *full line*, respectively) are shown to the *right*. The fitting parameters and details of the fitting procedure are listed in Table II. To decrease heavy atom scattering, the buffer for the EXAFS samples was changed to 20 mM BisTris, pH 7, by iterative use of Centricon devices (Millipore). The final protein concentration was ~2–3 mM. The free metal concentration was below 2 μM for the Zn_1 species and about 5 μM for the Zn_2 species. X-ray fluorescence was monitored with a 13-element Ge detector during an average time of 24 min/scan. Up to 30 scans/sample were averaged at a temperature of 25 K.

wild type, H88S, and C168S high affinity dissociation constants were almost the same (0.6, 0.4, and 0.6 nM, respectively). This suggests that both binding sites in the wild type enzyme show very similar affinities (microscopic dissociation constants), a fact that is supported by the distribution obtained from EXAFS, PAC, and absorption spectroscopy. At first glance

TABLE II

Results of theoretical EXAFS data analysis for wild type Zn_1- and Zn_2-BcII and Zn_2 species of the C168S and H210S mutants

The presented values correspond to the theoretical fits shown in Fig. 5. Two binding sites were introduced in the fitting process as independent clusters. Since minor deviations in the distance of identical ligand types cannot be separated with statistical reliability they were grouped. Thus the three histidines in the 3H site were not treated separately. Additionally, other first and second sphere scatterers were grouped in cases when a separate treatment was found to be unreliable as judged from the results of the calculated correlation matrices. Coordination numbers (N_i) were constrained to be integer values. This could be done since fitting of N_i for first shell ligands resulted in values deviating by <5% of the rounded given values. Ligand distances are given as R_i and Debye-Waller factors as σ^2. Histidine ligands were treated as imidazole units with the coordinating nitrogen atom as the one with the attached uncertainty. Debye-Waller factors were constrained (*e.g.* a^* was constrained to equal a). In the following the refined Fermi energy (EF), the resulting fit index (FI) and the R-factor (R) are given together with occupancy of sites and zinc-zinc distance.

enzyme	site	ligand	atom	N_i	R_i [Å]	σ^2 [Å^2]
Zn_1-BcII, wild type[A)]	3H-site	His	N	3	1.984 ± 0.009	0.00101 ± 0.00064 (b^*)
			C	3	2.925	0.01210 ± 0.00306 (a^*)
			C	3	3.005	0.01210 ± 0.00306 (a)
			C	3	4.086	0.02727 ± 0.01150 (c^*)
			N	3	4.090	0.02411 ± 0.00537 (d^*)
		H_2O/OH^-	O	1	1.750 ± 0.006	0.00102 ± 0.00209
		second sphere	O	2	2.970 ± 0.022	0.01210 ± 0.00306 (a^*)
	DCH-site	Cys	S	1	2.240 ± 0.0066	0.00379 ± 0.00210
		His	N	1	2.006 ± 0.025	0.00101 ± 0.00064 (b)
			C	1	2.749	0.01210 ± 0.00306 (a^*)
			C	1	3.155	0.01210 ± 0.00306 (a^*)
			C	1	3.988	0.02727 ± 0.01150 (c)
			N	1	4.140	0.02411 ± 0.00537 (d)
		$Asp/H_2O/OH^-$	O	2	1.884 ±0.0055	0.00230 ± 0.00189
		second sphere	O	2	3.374 ± 0.027	0.01210 ± 0.00306 (a^*)
Zn_2-BcII, wild type[B)]	3H-site	His	N	3	1.965 ± 0.005	0.0023 ± 0.0012
			C	3	2.867	0.0111 ± 0.0081 (f^*)
			C	3	3.016	0.0111 ± 0.0081 (f)
			C	3	4.045	0.0300 ± 0.0081 (g^*)
			N	3	4.080	0.0300 ± 0.00808 (e^*)
		H_2O/OH^-	O	1	1.743 ± 0.01	0.0033 ± 0.0024
		second sphere	O	3	3.351 ± 0.017	0.0078 ±0.0046
			O	2	4.239 ± 0.028	0.0100 ± 0.0076 (h^*)
	DCH-site	Cys	S	1	2.213 ± 0.006	0.0027 ± 0.0023
		His	N	1	2.094 ± 0.021	0.0074 ± 0.0126
			C	1	3.313	0.0111 ± 0.0081 (f^*)
			C	1	2.997	0.0111 ± 0.0081 (f^*)
			C	1	4.178	0.0300 ± 0.0081 (g)
			N	1	4.207	0.0300 ± 0.0080 (e)
		$Asp/H_2O/OH^-$	O	2	1.871 ± 0.007	0.0066 ± 0.0021
		second sphere	O	1	2.854 ± 0.032	0.0089 ± 0.0065
			O	1	4.239 ±0.028	0.0100 ± 0.0076 (h)
Zn_2-BcII, C168S mutant[C)]	3H-site	His	N	3	2.023 ± 0.005	0.00126 ± 0.00089 (j^*)
			C	3	2.730	0.01088 ± 0.00595 (k^*)
			C	3	3.189	0.01944 ± 0.00792 (l^*)
			C	3	3.979	0.02640 ± 0.00800 (n^*)
			N	3	4.157	0.01408 ± 0.00221 (m^*)
		H_2O/OH^-	O	1	1.733 ± 0.009	0.00223 ± 0.00113 (i^*)
		second sphere	O	3	2.957 ± 0.016	0.00318 ± 0.00144 (o^*)
	DSH-site	His	N	1	1.968 ± 0.016	0.00126 ± 0.00089 (j)
			C	1	2.895	0.01088 ± 0.00595 (k)
			C	1	3.011	0.01944 ± 0.00792 (l)
			C	1	4.117	0.02640 ± 0.00800 (n)
			N	1	4.031	0.01408 ± 0.00221 (m)
		$Asp/H_2O/OH^-$	O	2	1.854 ± 0.007	0.00496 ± 0.0014
		$Ser?/H_2O$	O	2	1.948 ± 0.009	0.00223 ± 0.00113 (i)
		second sphere	O	1	2.931 ± 0.050	0.00318 ± 0.00144 (o)
Zn_2-BcII, H210S mutant[D)]	3H-site	His	N	3	1.997 ± 0.005	0.00100 ± 0.00120
			C	3	2.772	0.0295 ± 0.0165
			C	3	3.129	0.030 ± 0.008
			C	3	4.1304	0.0149 ± 0.0021
			N	3	3.9997	0.030 ± 0.007
		H_2O/OH^-	O	1	1.688 ± 0.007	0.00219 ± 0.00189
		second sphere	O	3	2.934 ± 0.009	0.00779 ± 0.00280
	DCS-site	Cys	S	1	2.266 ± 0.005	0.0021 ± 0.00125
		$Asp/Ser/H_2O/OH^-$	O	3	1.871 ± 0.0039	0.0037 ± 0.00081
		chloride	Cl	1	2.151 ± 0.007	0.0074 ± 0.00211

A) The coordination number of the absorber was 0.48 for the first (3H site) and 0.52 for the second cluster (DCH site). No contribution of Zn-Zn scattering could be detected. EF = 0.2161 ± 0.1821 eV; FI = 1.403; R = 24.470%.

B) The coordination number of the absorber was fixed at 0.5 for both clusters representing two fully occupied sites. EF = 1.147 ± 0.175 eV; FI = 1.1317; R = 23.707%. The zinc-zinc distance is 3.701 ± 0.013 Å with a Debye-Waller factor of 0.0133 ± 0.0027 Å^2 constrained to be identical for both zinc ions.

C) The coordination number of the absorber was fixed at 0.5 for both clusters representing two fully occupied sites. EF = 0.2161 ± 0.18205 eV; FI = 1.403; R = 24.470%. The zinc-zinc distance is 3.617 ± 0.060 Å with a Debye-Waller factor of 0.0032 ± 0.00142 Å^2 constrained to be identical for both zinc ions.

D) The coordination number of the absorber was fixed at 0.5 for both clusters representing two fully occupied sites. EF = 0.360 ± 0.162 eV; FI = 0.876; R = 19.971%. The zinc-zinc distance is 3.705 ± 0.015 Å with a Debye-Waller factor of 0.017 ± 0.00344 Å^2 constrained to be identical for both zinc ions.

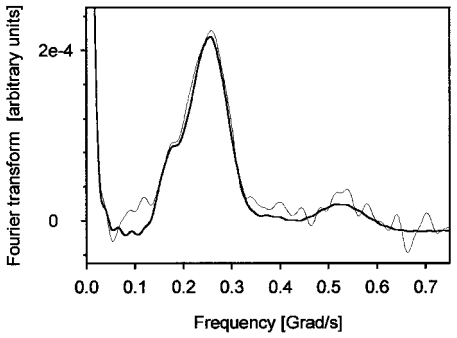

FIG. 6. **PAC spectrum of the ^{111m}Cd-substituted H88S mutant.** A solution containing about 10 pmol of ^{111m}Cd in H_2O was mixed with metal-depleted buffer containing additional cadmium ions. To this solution apoenzyme was added such that the final conditions were: 50 μM enzyme in 20 mM HEPES, 0.1 M NaCl, pH 7.1, and 10 μM total cadmium (= 0.2 equivalents). A 10-min waiting period allowing the metal to bind was included (at room temperature) before sucrose was finally added to give a 55% (w/w) solution. Within 10 min the sample was cooled to 1 °C. The sample volume was 50 μl. The PAC experiment was performed at 1 °C. The spectrum (*thin line*) represents the Cd_1 species. The theoretical fit (*thick line*) was obtained with two NQIs representing 30 and 70% occupation of two different ligand geometries. The corresponding NQI parameters are listed in Table III and are compared with data obtained with the wild type enzyme and the C168A mutant.

this seems contradictory because the binding of a second zinc ion would be governed by strongly increased dissociation constants (3 orders of magnitude) for both the wild type and the mutant enzymes. The difficulty in understanding this apparent contradiction comes from the view that a high and a low affinity macroscopic dissociation constant infers a high and a low affinity metal binding site. When assuming equal affinities for both sites, corresponding to equal microscopic dissociation constants, the weak affinity for a second zinc ion can only be explained in terms of negative cooperativity. A combination of NMR and PAC spectroscopy with the Cd(II)-substituted enzyme (9) led to the conclusion that an exchange of the metal ion between both binding sites occurs on a time scale of 0.1–10 μs. Thus, the mononuclear species cannot be considered as a system with one occupied and one free sites. An observation of the enzyme active site with a millisecond time scale (NMR) would give the impression of a delocalized metal ion rapidly exchanging between the two sites, whereas a nanosecond time scale (PAC) would reveal the occupation of the individual sites. If the exchange between the neighboring sites is fast, a successful docking of a second metal ion could be hindered significantly. In this respect the dynamics of the exchange would be responsible for the observed negative cooperativity. The modified electrostatics of the site after binding a first metal ion might also contribute to modified binding kinetics. However, the D90N mutant exhibits almost the same dissociation constants as the other mutants, although the attractive potential of a negatively charged carboxylate is removed.

A comparison of wild type and mutant enzymes shows that mutations of the zinc ligands barely affect the two dissociation constants. All three 3H-site mutants show a somewhat higher affinity for binding a second zinc ion (and a second Cd(II) ion to H88S) when compared with the wild type enzyme. This higher affinity could result because the substitution to serine increases the available space and thereby facilitates the binding of two metal ions. However, negative cooperativity still persists as the two macroscopic dissociation constants for these mutants differ by about three orders of magnitude. Fast exchange between the two metal sites for the mononuclear enzyme could thus also occur for these mutants. The H88S mutant PAC results demonstrate that the microscopic dissociation constants of both binding sites differ by a factor of less than 3 (Table III), whereas the high and low affinity dissociation constants differ by a factor of 300.

Our hypothesis that the low affinity for the binding of a second metal ion is related to the decreased association rate through mutual destabilization from the neighboring metal ion is confirmed by the kinetic studies of Cd(II) binding to the wild type enzyme. Whereas the binding of the first metal ion has an association rate constant $k_{on,1} = 26\ \mu M^{-1}\ s^{-1}$, the association of the second metal ion is 2 orders of magnitude slower and might be kinetically hindered because of the rapid exchange of the metal ion in the Me_1 species. The easier binding of a second equivalent to the 3H-site mutants compared with the wild type could thus be explained by a decelerated exchange rate between sites resulting in a better accessibility for docking the second metal ion. With a second metal ion bound, the Zn_2 species of wild type and mutants show almost identical structural characteristics with respect to Zn-Zn distance, presence of bridging hydroxide, and Zn-ligand distances as derived from EXAFS spectroscopy (Table IV).

Binding of Co(II) to Wild Type and Mutant Enzymes—The wild type enzyme binds the first Co(II) ion with a macroscopic dissociation constant of 93 nM (Fig. 2), 2 orders of magnitude higher than that of the first Zn(II) ion. The same ratio, between the two metal ions, is seen for the association rate constant ($k_{on,1}$). The affinity for Co(II) is thus two orders of magnitude weaker than for Zn(II) because of the lower value for the association rate $k_{on,1}$ for Co(II). The spectral features obtained at a [Co(II)]/[enzyme] ratio of 1 are identical to those described earlier (23). Increasing the [Co(II)]/[enzyme] ratio above 1 results in an additional charge transfer band at 383 nm. A well defined isosbestic point at 364 nm indicates two different Co(II) LMCT band positions, one for the mononuclear (344 nm) and one for the binuclear enzymes (383 nm). A stepwise addition of NaCl to the Co_2 species resulted in the disappearance of the LMCT band at 383 nm and increased the absorbance at 344 nm (data not shown), indicating that chloride hinders the binding of a second Co(II) ion.

The spectroscopic data presented here are partly in contradiction to those presented by Orellano *et al.* (24) who concluded that so-called "high" (3H site) and "low" (DCH site) affinity sites were occupied subsequently. The differences observed might result from the different conditions used. The work presented here was performed in a buffer for which no interaction with the enzyme or metal ion could be observed. The same spectral changes as described here were obtained in 15 mM sodium cacodylate, pH 7.0 (data not shown). Earlier studies were performed in succinate buffer at pH 6.3 (24) or in a cryosolvent containing 60% ethylene glycol in 80 mM sodium cacodylate, pH 6.4 (glass electrode reading in aqueous-organic solvent) (23). It might be assumed that solvent composition, the presence of succinate, and/or the lower pH are responsible for the different spectroscopic behavior. This assumption is supported by the recent finding that for the metallo-β-lactamase from *Pseudomonas aeruginosa* (IMP-1), which belongs to the same subclass as BcII, succinic acid is an inhibitor (25). Our dissociation constant for the first Co(II) ion is 3 orders of magnitude lower than the one published previously (24).

All mutant enzymes bind one equivalent of Co(II) with a rather high affinity (Table I). Variations of dissociation constants among mutants are larger than those obtained for zinc binding. The low dissociation constants found for the DCH-site mutants C168A and H210S relative to those found for the mutants of the 3H site suggest a preferential occupation of the 3H site for these mutants and the wild type. The absence of the sulfur-to-cobalt LMCT band in the H210S and the D90N mutants, except for some absorption between 320 and 425 nm, suggests that mutations in

TABLE III
NQI parameters for ^{111m}Cd-β-lactamase
The data for the H88S mutant were obtained from the fit shown in Fig. 6. For explanation of NQI parameters, refer to "Materials and Methods."

Species (reference)	[Cd]/[enzyme]	NQI	ω_0	η	δ	τ_r	Occupancy
			Mrad/s			*ns*	*%*
H88S	0.2	NQI-1	114 (±4)	0.73 (0.04)	0.10 (±0.01)	200 (±20)	30 (±4)
		NQI-2	153 (±2)	0.86 (±0.03)	–	–	70 (±4)
wild-type (9)	0.2	NQI-1	105 (±4)	0.69 (0.07)	0.15 (±0.02)	111 (±11)	46 (±10)
		NQI-2	158 (±4)	0.56 (±0.06)	–	–	54 (±10)
wild type (8)	<1	NQI-c3	149 (±9)	0.42 (0.04)	0.22 (±0.04)	72 (±12)	70 (±3)
		NQI-c4	84 (±11)	0.50 (±0.14)	–	–	30 (±3)
C168S (8)	<1	NQI-c4[a]	–	–	–	–	89 (±3)
		free Cd(II)	–	–	–	–	11 (±3)

[a] NQI parameters are like those obtained for the low frequency site of the wild type enzyme.

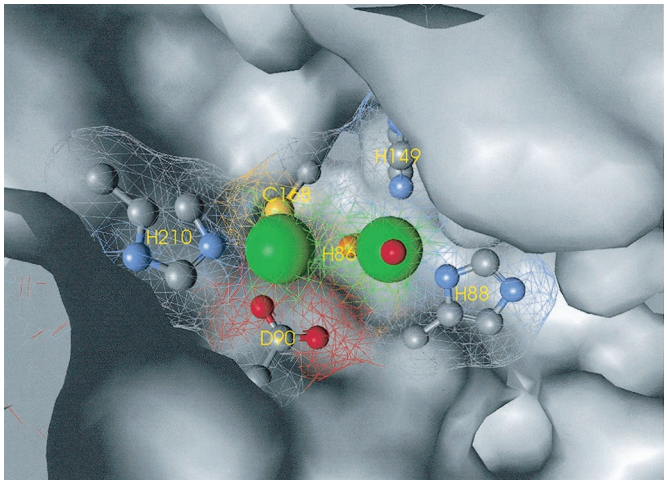

FIG. 7. **Surface representation of the substrate binding cleft of wild type BcII.** The solvent-accessible surface of the protein was calculated for the Zn_2-BcII structure file, 1BVT (3), with a 1.4-Å probe, excluding the metal ions and the zinc ligands, and is represented in *gray*. The solvent-accessible surface of the zinc ions (van-der-Waals radii shown in *green*) and the zinc ligands (*ball-and-stick* models) was calculated separately to allow representation with a mesh surface. His^{86} (shown in *orange*) is located behind the 3H-site zinc ion and does not contribute to the solvent-accessible surface. The zinc-bound water in 1BVT is represented as a *red sphere*.

the DCH site further shift the preference to the 3H site (Fig. 3).

All 3H-site mutants show a pronounced LMCT band around 345 nm. The highest intensity for this band is obtained for the H88S mutant, a slightly lower intensity for the H149S mutant, and a wild type-like intensity for the H86S mutant (Table II). Interestingly, His^{86} is the residue substituted by Asn in subclass B2, and in all x-ray structures of BcII obtained at low pH the distance from His^{86} to the zinc ion from His^{86} is longer than that from His^{88} and His^{149} (see Table IV). Surprisingly, none of the mutant enzymes except H149S shows ϵ values comparable with that of the wild type in the d-d region of the spectra. The DCH-site mutants show the same band positions in the d-d region (second derivatives in Fig. 3, *E–G*), as the wild type, dominated by a maximum around 550 nm and weaker shoulders between 600 and 650 nm and between 450 and 500 nm, suggesting that the d-d region represents characteristics of an occupied 3H site. Although all spectra of the 3H-site mutants show LMCT bands with varying intensities, the band positions in the d-d region are different. Nevertheless, one would expect the d-d band contribution from the 3H-site mutations to be dominated by the DCH-site occupation. Therefore, it might be concluded that a DCH-site occupation contributes to the d-d region with only very low ϵ values as expected for pentacoordinated Co(II). The features observed for the 3H-site mutants would then also reflect occupation of the modified 3H site. The largest variation of band positions in the d-d region is observed for the H149S mutant. Because the [Co(II)]/[enzyme] stoichiometry is 1, the LMCT band would then represent only a partial occupation of the DCH site, indicating a distribution of Co(II) between both binding sites as it has been shown earlier for Cd(II)-binding to the wild type enzyme (8).

The more intense LMCT bands of the 3H-site mutants H88S and H149S seem to indicate an increased occupancy of the DCH site compared with the wild type. However, from the spectroscopic data alone it seems impossible to calculate relative occupancies. Only direct methods such as PAC and EXAFS spectroscopy allow quantification of relative occupancies.

Perturbed Angular Correlation of γ-Ray Spectroscopy of the Cd(II)-substituted H88S Mutant—A PAC spectrum from the C168A mutant exhibited a pure 3H-site geometry (8), whereas the PAC spectrum from the H88S mutant (Fig. 6) was characterized by 2 NQIs (Table III), showing the co-existence of two different ligand geometries for the mononuclear mutant (only 0.2 equivalents of Cd(II) were available per enzyme molecule). As can be inferred from the dissociation constants, affinity for the second cadmium ion is orders of magnitude lower than for the first one (Table I). Thus, when bound to the H88S mutant Cd(II) is distributed between the unmodified DCH site and the modified 3H site. The dominating high frequency NQI with ω_0 = 153 Mrad/s could be identified as the DCH site by comparison with spectra obtained earlier for the wild type and the C168A mutant (Table IV). The other NQI with an occupancy of 30% would then be assigned to the 3H site, now with a His to Ser substitution. Slight differences occur among the different NQIs, suggesting sensitivity to both the exact conditions for the PAC experiments and the mutation.

EXAFS Spectroscopy Versus X-ray Crystallography in Defining Metal Ion Environments—Here we present for the first time a detailed analysis of EXAFS spectra for both Zn_1- and Zn_2-BcII 569/H/9 wild type and the Zn_2 species of the C168S and H210S mutants. A previous EXAFS investigation of the Zn_1 enzyme from strain 5/B/6 resulted in a coordination number of about 0.5 for a cysteine sulfur, suggesting a distribution of zinc ions between the two sites (5). To allow a direct com-

TABLE IV

Comparison of Zn-ligand distances [Å] obtained by EXAFS spectroscopy to distances obtained by x-ray crystallography

The structural parameters were obtained from the coordinate files given. Crystallization conditions for BcII were: pH 5.6 for 1BMC (2), pH 5.6 for 1BVT (3), pH 5.2 for 1BC2 (4), pH 5.6 for BcII (pH 7.5), but crystals were dropped into HEPES pH 7.5 before freezing (8), and pH 5.6 for the C168S mutant 1DXK (26). The structural parameters for the enzymes from *B. fragilis* (CcrA) and *Stenotrophomonas maltophilia* (L1) (27) are shown also. Crystals used for determining the CcrA structures 1ZNB (28) and 1BMI (29) were grown at pH 7.5 and 9, respectively.

		EXAFS data				Crystallographic data PDB accession codes				
						1BMC	1BVT 1BC2, A 1BC2, B BcII (pH7.5)	1DXK	1ZNB,A 1ZNB,B 1BMI,A 1BMI,B	1SML
site	organism	BcII							CcrA	L1
	species	Zn_1-WT	Zn_2-WT	Zn_2-C168S	Zn_2-H210S	Zn_1-WT	Zn_2-WT	Zn_1-C168S	Zn_2-WT	Zn_2-WT
	ligand									
3H-site	H86-N	1.98 (±0.01)	1.97 (±0.01)	2.02 (±0.01)	2.00 (±0.01)	2.47	2.19 2.27 2.24 2.04	2.10	2.14 2.22 2.13 2.11	2.03
	H88-N					2.38	2.15 1.95 2.16 2.06	2.06	2.07 2.16 2.07 2.06	2.11
	H149-N					2.37	2.09 2.00 2.11 2.07	2.04	2.08 2.01 2.06 2.08	2.05
	H_2O/OH^-	1.75 (±0.01)	1.74 (±0.01)	1.73 (±0.01)	1.69 (±0.01)	-	2.09 1.90 1.90 2.19	2.26	1.88 1.97 1.78 1.88	1.88
DCH-site	C168-S	2.24 (±0.01)	2.21 (±0.01)		2.27 (±0.01)	-	2.38 1.91 1.98 2.15	-	2.30 2.35 2.42 2.40	
	S168-O			1.95? (±0.01)						
	H168-N									2.02
	H210-N	2.01 (±0.03)	2.09 (±0.02)	1.97 (±0.02)		-	2.21 2.59 2.45 2.25	-	2.10 2.20 2.01 2.07	2.07
	S210-O				1.87 (±0.01)					
	D90-O	1.88 (±0.01)	1.87 (±0.01)	1.85 (±0.01)	1.87 (±0.01)	-	2.28 2.75 2.91 2.15	-	2.25 2.15 2.16 2.07	2.07
	H_2O/OH^-					-	3.73 2.48, 2.55 2.70, 3.06 2.19	-	2.06, 2.27 2.13, 2.18 1.89, 2.21 1.86, 2.24	2.06
Zn-Zn distance		-	3.70 (±0.01)	3.62 (±0.06)	3.70 (±0.02)	-	3.82 3.85 4.37 3.94	-	3.47 3.46 3.44 3.47	3.46

parison with available crystallographic data, the investigation presented here was performed with the enzyme from strain 569/H/9. The high quality of the fits allows a direct comparison with x-ray crystallographic data (Table IV).

A comparison of x-ray structural data obtained for BcII shows an apparent variation in ligand-to-metal distances that is not found to a similar extent in different structures derived from the *B. fragilis* enzyme (CcrA) (Table IV). This feature of BcII was discussed in terms of a less well defined coordination sphere (4). The most obvious difference between the conditions of the x-ray diffraction experiments from which the structures of BcII and CcrA were derived concerns the pH used to grow the

crystals. Whereas CcrA was crystallized at neutral (28) or basic pH (29), all BcII crystals were grown in citrate buffer at pH 5.6 (2, 3, 8) or in Tris solution at pH 5.2 (4). We have shown earlier that the crystallization conditions used were such that the enzyme did not retain two zinc ions (5). Thus, it might be suspected that the two binding sites were not fully occupied in the low pH structures. An important hint concerning the role of pH comes from a comparison of the structures published earlier (3, 4) with those obtained after dropping crystals grown at pH 5.6 into HEPES, pH 7.5, before flash cooling (8). Modifications of all ligand-metal bond lengths were then observed in both binding sites (see Table IV). Under the assumption of partly occupied sites, Zn_1 and Zn_2 species might coexist in the crystals, as discussed by Carfi *et al.* (3). Slightly differing ligand positions in occupied and unoccupied sites have been observed by comparison with a structure of the metal-free enzyme (3). Distribution of zinc between the two sites in the Zn_1 enzyme would result in average electron densities. When using these densities for model building, incorrect positions of residues lying between the "real" positions in occupied and unoccupied sites could result. This should lead to increased temperature factors for the corresponding residues. In the structure obtained by Fabiane *et al.* (4) (PDB accession code 1BC2), the temperature factors for both zinc positions were calculated under the assumption of fully occupied sites resulting in 31–32 $Å^2$ and 53–62 $Å^2$ for the 3H and the DCH site, respectively. For an electron-rich atom like Zn(II) these values appear rather high, particularly for the DCH site, when compared with the average temperature factor of 29.8 $Å^2$ for all protein atoms (4).

In contrast to the data from x-ray crystallography, unoccupied sites do not contribute to the data in EXAFS spectroscopy. Another advantage is the nearly physiological pH (pH 7.0) at which the EXAFS measurements were performed. The low pH used for the crystallographic studies could have affected the protonation state of residues in the active site. Protonation of cysteine could for instance influence the distribution of zinc between both binding sites, leading to a preference for the 3H site.

The EXAFS spectrum of Zn_1-BcII wild type at pH 7.0 results in two equally populated sites (Table IV), which is in agreement with data obtained for the enzyme from strain 5/B/6 (5). The independent analysis of EXAFS data for Zn_1 and Zn_2 wild types as well as the C168S and H210S mutants resulted in highly conserved ligand-metal distances varying by less than 0.1 Å (Table IV). This finding is in contradiction with the published crystallographic data showing a high variability of ligand distances, especially in the DCH site of BcII. Disregarding the first BcII structure described (2) (PDB accession code 1BMC), the average distance of a histidine nitrogen to zinc in the 3H site in all available structures is 2.097 ± 0.070 Å compared with 1.993 ± 0.019 Å obtained by EXAFS. In the EXAFS analysis the three histidines of the 3H site were grouped, resulting in a standard deviation of less than 0.01 Å for the average distance of all investigated species, whereas the distance derived from x-ray data varies by up to 0.3 Å, reflecting in part the larger uncertainty resulting from analysis of x-ray data compared with analysis of EXAFS data. This suggests that an occupied 3H site shows a well defined ligand geometry. Thus, the variation in the x-ray structures likely reflects partial occupation of the site in BcII. This argument also applies to the DCH site where the variation in metal-to-ligand distances, derived from x-ray diffraction, is even more pronounced (see Table IV).

In all EXAFS spectra, including Zn_1 wild type BcII, a zinc-ligand distance of 1.73 ± 0.03 Å is found in the 3H site. This ligand is most likely a hydroxide ion. Only one x-ray structure (1BMI/A) shows such a short distance (29). Perhaps the choice of distance constraints for metal ion-bound hydroxides should be reconsidered in crystallographic refinements. The distances obtained for the carboxylate oxygen of Asp^{90} and the first shell water molecule cannot be distinguished but gave an average value of 1.86 ± 0.01 Å. The value of this distance and the number of oxygen ligands at this distance (see Table II) support the hypothesis that a bridging hydroxide ion occurs in the Zn_2 species of wild type and both mutants.

The zinc-zinc distance derived from EXAFS spectroscopy for the wild type BcII is 3.70 Å and thus does not deviate significantly from the average value obtained from crystallographic studies (4.0 ± 0.2 Å). The H210S mutant shows exactly the same zinc-zinc distance as the wild type, whereas the C168S mutant is characterized by a slightly decreased value, possibly because of the absence of one negatively charged ligand.

In addition to the conserved zinc-zinc distance, the mutations had little influence on the ligand distances as derived by EXAFS spectroscopy. The H210S mutant shows a modified ligand sphere in the DCH site because of the binding of chloride, which could be identified in the fitting process. This could arise from an active site cavity of increased size for the H210S mutant creating space for the coordination of a bulky chloride ion (see Fig. 7).

Conclusions—The controversial discussion of mono- and binuclear catalytic mechanisms for metallo-β-lactamases was initiated by the nearly simultaneous availability of x-ray structures for the assumed mononuclear enzyme BcII (2) and the binuclear enzyme from *B. fragilis* (28). The structural comparison suggested that the binding site of zinc in the first BcII structure published represented the "high affinity site." In most of the subsequent publications this interpretation persisted, leading to the conclusion that only the 3H site was necessary for catalytic activity in mononuclear metallo-β-lactamases (see Ref. 22).

The present investigation contributes new insights with respect to this discussion. It can be concluded that the metallo-β-lactamase from *B. cereus* does not contain a high and a low affinity metal ion binding site. The first metal ion, bound with a low dissociation constant, is distributed between both available binding sites. In case of the Zn_1 wild type enzyme, both sites are more or less equally populated. A distribution of a single metal ion between both binding sites is also observed in the wild type (8) and H88S mutant of the mononuclear cadmium enzyme, in many mutants, and in the wild type of the mononuclear cobalt enzyme. In cryoenzymological studies of the Co(II)-substituted enzyme, Bicknell and Waley (23) observed a reaction intermediate with a 7-fold increased LMCT band intensity when compared with the resting enzyme. Considering that these studies might have been performed on the Co_1 enzyme, an alternative interpretation to the view of these authors (23) could be given. The increased LMCT band intensity after binding benzylpenicillin might reflect a modified binding site preference for the metal ion during catalysis, which supports a functional importance of both metal ion binding sites in the mononuclear enzyme. Summarizing the accumulated experimental evidence, it seems unjustified to disregard the potentially functional importance of DCH site occupancy in the mononuclear enzyme.

The mutational study clearly shows that none of the mutations prevents the binding of a second metal ion. Furthermore, the dissociation constant for formation of the binuclear enzyme is in some cases even lower than that for the wild type. The negative cooperativity of metal ion binding inferred in this work seems to be independent of the ligand mutations. The data from the mutant enzymes show that binding of two zinc

ions occurs in an almost unmodified geometry when compared with the wild type. The reason for the negative cooperativity is found in the strongly modified kinetics of metal ion binding for the apo- and mono-Zn enzymes. The affinity for the binding of an additional metal ion to the mono-Zn enzyme is decreased primarily because of the strongly decreased association rate constant of the metal ion. In the light of recently obtained evidence for the dynamics of metal ion exchange between both binding sites (9), the rapid exchange in the mononuclear enzyme would probably impede the successful approach of a second metal ion.

Acknowledgments—We thank Dr. B. Wannemacher for help with the atomic absorption measurements and Marianne Lund Jensen for excellent laboratory work during the PAC experiments.

REFERENCES

1. Galleni, M., Lamotte-Brasseur, J., Rossolini, G. M., Spencer, J., Dideberg, O., and Frère. J.-M. (2001) *Antimicrob. Agents Chemother.* **45,** 660–663
2. Carfi, A., Pares, S., Duée, E., Galleni, M., Duez, C., Frère, J.-F., and Dideberg, O. (1995) *EMBO J.* **14,** 4914–4921
3. Carfi, A., Duee, E., Galleni, M., Frere, J. M., and Dideberg, O. (1998) *Acta Crystallogr. Sect. D Biol. Crystallogr.* **54,** 313–323
4. Fabiane, S. M., Sohi, M. K., Wan, T., Payne, D. J., Bateson, J. H., Mitchell, T., and Sutton, B. J. (1998) *Biochemistry* **37,** 12404–12411
5. Paul Soto, R., Bauer, R., Frère, J.-M., Galleni, M., Meyer-Klaucke, W., Nolting, H. F., Rossolini, G. M., de Seny, D., Hernandez Valladares, M., Zeppezauer, M., and Adolph, H. W. (1999) *J. Biol. Chem.* **274,** 13242–13249
6. Paul Soto, R., Hernandez Valladares, M., Galleni, M., Bauer, R., Zeppezauer, M., Frère, J.-M., and Adolph, H. W. (1998) *FEBS Lett.* **438,** 137–140
7. Wang, Z., Fast, W., Valentine, A. M., and Benkovic, S. J. (1999) *Curr. Opin. Chem. Biol.* **3,** 614–622
8. Paul Soto, R., Zeppezauer, M., Adolph, H. W., Galleni, M., Frère, J.-M., Carfi, A., Dideberg, O., Wouters, J., Hemmingsen, L., and Bauer, R. (1999) *Biochemistry* **38,** 16500–16506
9. Hemmingsen, L., Damblon, C., Antony, J., Jensen, M., Adolph, H. W., Wommer, S., Roberts, G. C. K., and Bauer, R. (2001) *J. Am. Chem. Soc.* **123,** 10329–10335
10. Teo, B. K. (1986) *EXAFS: Basic Principles and Data Analysis*, Springer, Berlin
11. Meneghini, C., and Morante, S. (1998) *Biophys. J.* **75,** 1953–1963
12. Hernandez Valladares, M., Felici, A., Weber, G., Adolph, H. W., Zeppezauer, M., Rossolini, G. M., Amicosante, G., Frère, J.-M., and Galleni, M.(1997) *Biochemistry* **36,** 11534–11541
13. Hernandez Valladares, M., Kiefer, M., Heinz, U., Paul Soto, R., Meyer-Klaucke, W., Nolting, H. F., Zeppezauer, M., Galleni, M., Frère, J.-M., Rossolini, G. M., Amicosante, G., and Adolph, H. W. (2000) *FEBS Lett.* **467,** 221–225
14. Simons, T. J. B. (1993) *J. Biochem. Biophys. Methods* **27,** 25–37
15. Lee, P. A., and Pendry, J. B. (1975) *Phys. Rev. B* **11,** 2795–2811
16. Gurman, S. J., Binsted, N., and Ross, I. (1984) *J. Phys. Chem.* **17,** 143–151
17. Hedin, L., and Lundqvist, S. (1969) *Solid State Phys.* **23,** 1–181
18. Joyner, R. W., Martin, K. J., and Meehan, P. (1987) *J. Phys. C Solid State Phys.* **20,** 4005–4012
19. Hemmingsen, L., Bauer, R., Bjerrum, M. J., Adolph, H. W., Zeppezauer, M., and Cedergren-Zeppezauer, E. (1996) *Eur. J. Biochem.* **241,** 546–551
20. Bauer, R., Danielsen, E., Hemmingsen, L., Sørensen, M. V., Ulstrup, J., Friis, E. P., Auld, D. S., and Bjerrum, M. J. (1997) *Biochemistry* **36,** 11514–11524
21. Bauer, R. (1985) *Q. Rev. Biophys.* **18,** 1–64
22. Bounaga, S., Laws, A. P., Galleni, M., and Page, M. I. (1998) *Biochem. J.* **331,** 703–711
23. Bicknell, R., and Waley, S. G. (1985) *Biochemistry* **24,** 6876–6887
24. Orellano, E. G., Girardini, J. E., Cricco, J. A., Ceccarelli, E. A., and Vila, A. J. (1998) *Biochemistry* **37,** 10173–10180
25. Toney, J. H., Hammond, G. G., Fitzgerald, P. M. D., Sharma, N., Balkovec, J. M., Rouen, G. P., Olson, S. H., Hammond, M. L., Greenlee, M. L., and Gao, Y.-D. (2001) *J. Biol. Chem.* **276,** 31913–31918
26. Chantalat, L., Duee, E., Galleni, M., Frere, J. M., and Dideberg, O. (2000) *Protein Sci.* **9,** 1402–1406
27. Ullah, J. H., Walsh, T. R., Taylor, I. A., Emery, D. C., Verma, C. S., Gamblin, S. J., and Spencer, J. (1998) *J. Mol. Biol.* **284,** 125–136
28. Concha, N. O., Rasmussen, B. A., Bush, K., and Herzberg, O. (1996) *Structure* **4,** 823–836
29. Carfi, A., Duée, E., Paul-Soto, R., Galleni, M., Frère, J.-M., and Dideberg, O. (1998) *Acta Crystallogr. Sect. D Biol. Crystallogr.* **54,** 47–57